Geometric Optimization of Coreholder Head Designs in Coreflooding Experiments Using CFD

Murilo Guimarães Morimoto[1*], *Nicolas* da Silva Riva[1], *Cláudia Míriam* Scheid, *Luís* Américo Calçada[1], *Cristiano* Agenor Oliveira de Araujo[1], *André Luiz* Martins Compan[2], *Luiz Augusto* da Cruz Meleiro[1], and *Filipe* Arantes Furtado[1].

[1]Laboratório de Escoamento de Fluidos Giulio Massarani (LEF), R. UJ UFRRJ, Seropédica, Rio de Janeiro – RJ, 23890-000, Brazil
[2]Petróleo Brasileiro S.A./Petrobras, Rio de Janeiro, Brazil

Abstract. To better forecast the reservoir's oil production and appropriately employ recovery strategies, it is fundamental to quantify the phases' fractions within the rock accurately and how they interact. Such information can be gathered through petrophysical analysis using instruments such as the coreholder. However, because of the expensive alloys used in coreholder construction and the time required for multiple analyses, building different devices to study how their geometry influences multiphase flow may be economically infeasible. This research numerically investigated how oil in the core can be displaced by brine under various configurations of coreholder heads. The assessment was conducted using the Finite Volume Method (FVM), and multiphase flow and interface tracking were solved using the Volume of Fluid (VOF) algorithm. The coreholder's head geometric parameters evaluated were the gutter's width and the inlet orifice diameter. They were combined using a three-level factorial design of experiments. The results showed that the head's geometric layout can significantly reduce the oil saturation near the core inlet. At 3 mm from the core's inlet, it is possible to remove 65.19% more oil if the gutter's width increases from the minimum to the maximum levels studied.

1 Introduction

Coreflooding experiments are fundamental for obtaining better information on the petrophysical properties of an oil field [1]. Based on data from these studies, it is possible to estimate the amount of oil that could be obtained from the reservoir [2]. Moreover, coreflooding findings can help operators evaluate which exploration strategy would yield the maximum amount of oil or gas recovered while expending fewer resources. Hence, the study of multiphase flow within a core plug performed in coreholders is a key point in reservoir engineering.

The injection of brine into a core containing oil and brine in its connate saturation is also known as waterflooding. This process is part of determining the relative permeability of the phases in the core and the oil volume that can be produced [3]. In this experiment, water is injected into one face of the core plug, creating a front flow that pushes oil toward the outlet. At the end of the process, however, residual oil is expected to remain within the reservoir rock.

Several parameters can influence the fluid dynamics of brine in the core, including wettability, injection rate, chemical additives, and the device geometry [4–6]. Therefore, understanding and controlling these variables are vital for obtaining trustworthy results suitable for field analysis.

The homogeneity of the front flow is important for effectively sweeping oil across the core. If this homogeneity is breached, a large phase gradient would form within the core, leaving substantial portions of oil unswept. Consequently, a larger-than-expected oil residual saturation would be achieved. Therefore, it leads to an underestimation of an oil field's real production potential. To minimize the formation of an uneven front flow, the injection of brine into the core should be done evenly across the core's face rather than at a single point.

The segment of the coreholder responsible for distributing brine across the core's face is the coreholder's headpiece or head diffuser. Typically, this section may contain several gutters that intersect, forming a lattice. Several inlet diffuser geometries can be found in the literature, including designs with groove patterns that form squares, spirals, or a half-moon configuration [7]. The geometry of the headpiece can influence phase saturation in the core [8]. Therefore, it is important to equip the coreholder with a suitable headpiece to favor oil sweep by providing a homogeneous front flow and a small phase gradient.

Coreflooding experiments may use high-salinity brine and operate at high temperatures, which favor material corrosion [9,10]. Therefore, coreholders and their metallic accessories should be manufactured from special-grade alloys containing nickel, chrome, and molybdenum, which can be expensive [9]. Hence, constructing different headpieces to evaluate the homogeneity of the front flow may require significant resources. Therefore, the construction of headpieces that do not yield experimental gain should be avoided. To overcome this inconvenience

* Corresponding author: morimoto@ufrrj.br

and study the influence of several inlet diffuser geometries, numerical methods can be used to simulate the multiphase flow within the coreholder.

Numerical analyses are commonly used in petrophysical research [11]. When properly implemented, numerical studies enable the investigation of the occurrence and dynamics of viscous fingerings [12]. Moreover, it is also possible to foresee the volume of oil produced using enhanced oil recovery techniques with surfactants [13]. Furthermore, the mechanisms of the enhanced oil recovery using ion-tuned (smart water) can be detailed [14]. Lastly, the relative permeability of the phases within the core plug can also be numerically determined [3]. However, few studies in the literature elucidate how the coreholder's configuration and its accessory designs can alter phase displacement.

Hence, in this study, the groove width and the inlet diameter of a commercial headpiece were altered using the design of experiments. This allowed an investigation of how changes in the head diffuser geometry can alter the fluid-dynamics phases within the core.

2 Numerical implementations

2.1 Governing equations and considerations

In this numerical work, the Finite Volume Method (FVM) was employed. The governing differential transport equations were approximated as algebraic equations within a small control volume and then solved [15] using the software *ANSYS Fluent®*.

The Volume of Fluid (VOF) model was chosen to describe multiphase flow in the coreholder, as it is commonly employed in computational analyses of multiphase flow in porous media [3,12,16–19]. The main advantage of this approach is the consistent tracking of the interface between immiscible phases, which is ideal given that viscous fingering may develop in the core [20]. In this approach, each "*q*" phase has its own mass balance, assuming they are immiscible and do not interpenetrate; the continuity equation can be simplified to Equation 1.

$$\frac{\partial\left(\alpha_q \rho_q\right)}{\partial t} + \nabla \cdot \left(\alpha_q \rho_q \mathbf{v}\right) = 0 \tag{1}$$

where α_q and ρ_q are the volume fraction and the density of phase q, respectively, and $\mathbf{v}$ is the phase velocity.

The phase's velocity distribution across the computational domain is obtained when solving the momentum equation (Equation 2). In this numerical study, the interfacial tension arising from attractive forces between the components of the mixture was accounted for using the Continuum Surface Force (CSF) model of Brackbill, Kothe, and Zemach [21]. This consideration is represented as the third-to-last term of Equation 2.

$$\frac{\partial(\rho \mathbf{v})}{\partial t} + \nabla \cdot (\rho \mathbf{v}\mathbf{v}) = -\nabla P + \nabla \cdot \left[\mu\left(\nabla \mathbf{v} + \nabla \mathbf{v}^T\right)\right] + \\ + \rho \mathbf{g} + \sigma \frac{\rho \kappa \nabla \alpha_q}{0.5\left(\rho_q + \rho_r\right)} + \mathbf{S} + \mathbf{F_C} \tag{2}$$

where the density and viscosity of the mixture are represented as ρ and μ, respectively. P and $\mathbf{g}$ are the pressure and gravity, respectively. σ is the interface tension, which was deemed constant. ρ_r is the density of phase r. κ is the curvature of the interface. $\mathbf{S}$ is a source term representing the momentum sequestration in the porous media, and $\mathbf{F_C}$ is the influence of the capillary action on the flow.

In this research, the pores' gorges and the pores themselves were not described in the computational domain. Therefore, the momentum equations of cells in the free-flow zone (within the headpieces) and in the porous zone (within the core) differ; in the latter, the cell's momentum equation is described as Equation 2. In contrast, for cells in the headpieces, the last three terms of Equation 2 are defined as zero. This approach, also known as the Porous Media Model, is commonly used to model flow in permeable materials [22].

The moment loss within the core can be modeled using the Forchheimer-Darcy Equation, which accounts for viscous and inertial resistances [23]. However, in this study, it was assumed that a Darcy flow is established within the core, since the injection rate of pure brine is 1 cm^3/min, indicating that the losses due to viscous resistance are considerably higher than those due to inertial effects. Therefore, the **S** term of Equation 2 can be modeled as shown in Equation 3.

$$\mathbf{S} = -\frac{\mu}{K_{UDF,q}} \mathbf{v} \tag{3}$$

where K_{UDF} is the effective permeability of a generic phase "*q*".

In a multiphase flow within a porous medium, one phase can interfere with the flow of another; therefore, to properly describe these dynamics, it is crucial to account for each phase's effective permeability. This phenomenon can be modeled using relative permeability models [21], which were calculated in this study using the Corey model [25]. Hence, the relative permeability of the wetting brine phase can be modeled as in Equation 4. On the other hand, the relative permeability of the oil phase is described in Equation 5. Lastly, the normalized water saturation is presented in Equation 6.

$$K_{r,W} = K_{W,o}\left(\bar{S}^{N_W}\right) \tag{4}$$

$$K_{r,O} = K_{O,o}\left(1 - \bar{S}\right)^{No} \tag{5}$$

$$\bar{S} = \frac{S_W - S_{WI}}{1 - S_{WI} - S_{OR}} \tag{6}$$

where $K_{W,o}$ and $K_{O,o}$ are the referential relative saturation of brine (assessed at the irreducible water saturation (S_{WI})) and oil (evaluated at the residual oil saturation (S_{OR})), respectively. N_W and N_O are fitting parameters.

The influence of capillary action on fluid dynamics may be incorporated into the momentum equation. One approach is to model this influence as the negative of the capillary pressure gradient [24]. To simplify the model and save computational time, the capillary pressure gradient was assessed numerically as the ratio of the capillary pressure, modeled according to the Brooks-Corey Model [25], to a characteristic dimension defined as the square root of the absolute permeability [23,26]. This estimation is presented in Equation 7.

$$\mathbf{F}_C = -\nabla P_C \approx -\frac{P_C}{\sqrt{k}} = \frac{P_e \bar{S}^{-\frac{1}{\lambda}}}{\sqrt{k}} \quad (7),$$

where P_C is the capillary pressure, k is the absolute permeability, P_e and λ are parameters of the Brooks-Corey Model, which were assessed using the experimental data of Santos et al. (2021) [27].

2.2 Validation data

The numerical approach was validated using experimental data published by Santos *et al*. (2021) [27], some of which are presented in Table 1. Although Santos *et al*. (2021) [27] did not provide relative permeability data for the phases, their experimental data could be fitted nonlinearly to a Corey model. The results of this parameter estimation are presented in Table 2. This procedure was also used to evaluate the coefficients for modeling the capillary pressure, yielding P_e = 4100 Pa and λ = 2.66. Finally, the oil production of the sample analyzed by Santos *et al.* (2021) [27] reached a constant value within one hour after pure brine injection at a flow rate of 1 cm^3/min, and the pressure drop stabilized at 26.61 kPa.

Table 1. Experimental data of Santos *et al*. (2021) [27].

Parameter	Value
Core dimensions	Length: 4.78 cm Diameter: 3.82 cm
Core porosity	0.225
Core permeability	597 mD
Brine properties	Density: 1142 kg/m^3 Viscosity: 1.48 cP
Oil properties	Density: 856 kg/m^3 Viscosity: 23 cP

Table 2. Parameters of relative permeability of Corey model.

Parameter	Value
$K_{W,o}$	0.07
N_W	2.63
$K_{O,o}$	0.8995
N_O	1.34
S_{WI}	0.20
S_{OR}	0.2767

In this numerical study, the imbibition procedure, as well as the core and fluid properties adopted to investigate the influence of the coreholder head on the flow dynamics within the plug, were based on the experimental study of Santos *et al*. (2021) [27]. Hence, the contents of Tables 1 and 2 were used as input parameters for the numerical simulation. Therefore, the proposed model reproduces a multiphase flow using fluid and rock properties representative of those commonly encountered in reservoir engineering.

In this numerical study, it was assumed that the core's absolute permeability and porosity were constant throughout the computational domain. Furthermore, the initial condition considered that the brine was uniformly distributed within the core at its irreducible saturation (20%).

2.3 Spatial domain

2.3.1 Design of experiments

In this research, the effect of altering the design of a commercial coreholder's headpiece on the fluid dynamics of the phase distribution in the core was evaluated. The original inlet diffuser was modeled according to the one manufactured by *JBV – Usinagem Tecnologia Ltda.* and is named Spiderweb in this study. Its design and original dimensions are shown in Figure 1, which also highlights the brine inlet orifice in blue and the gutters of the headpiece in gray, where the injected fluids are allowed to flow. Lastly, it is important to note that the white areas in Figure 1 do not belong to the head mandrel; they serve merely as a contrast to highlight the gutters of the headpiece.

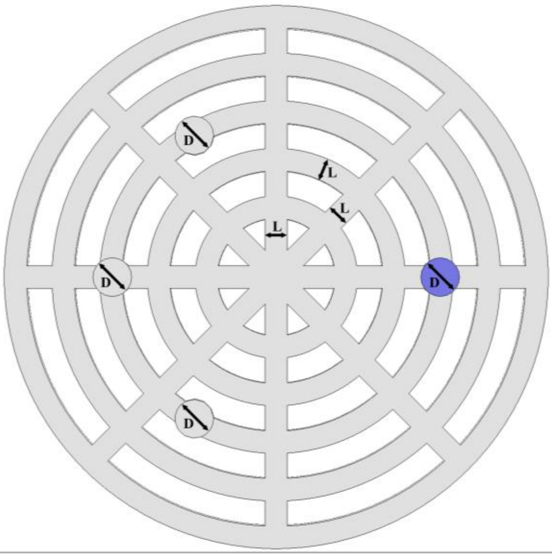

Dimension	Value (mm)
D	2.60
L	1.50

Fig. 1. Details of the Spiderweb inlet diffuser design and its original dimensions.

The Spiderweb headpiece is composed of 5 concentric rings connected by 8 gutters that radiate from the geometry's origin. The widths of the gutters and the rings are 1.50 mm. On the other hand, the inlet diameter and other detailed circular zones of Figure 1 were measured as 2.60 mm. Moreover, the depth of the grooves in this headpiece was measured at 0.65 mm, a feature shared by all other geometries developed in this paper.

In this study, the influence of channel width, the inlet orifice diameter, and other circular details was evaluated using a three-level factorial design; the combination of Design of Experiments with computational fluid dynamics analysis is suitable for understanding how changing parameters can alter flow mechanisms and how they affect one response of interest [28–30].

The channel's width and inlet diameter are coded as X_1 and X_2, respectively. The factorial design using coded variables is shown in Table 3, which lists all possible combinations of the geometry levels. The relationship between the coded variables and their real values is presented in Table 4. In this analysis, the coreholder equipped with the commercial headpiece, Spiderweb, is associated with study 6 in Table 3.

After each experimental run, the oil saturation in cross sections near the inlet (at distances of 3 mm, 5 mm, and 10 mm from the inlet) was fit to performance equations to examine its correlation with the assessed geometric parameters. Hence, a multiple regression technique was employed. The significance of each parameter was assessed based on its *p-value*, with a significance level of 10%.

Table 3. Three-level factorial design of experiment.

Study case	Channels width (X_1)	Inlet diameter (X_2)
1	– 1	– 1
2	– 1	0
3	– 1	+1
4	0	– 1
5	0	0
6	0	+ 1
7	+ 1	– 1
8	+ 1	0
9	+ 1	+ 1

Table 4. Codification of variables used in this work.

	– 1	0	+1
Channel's width (mm)	1.00	1.50	2.00
Inlet diameter (mm)	1.80	2.20	2.60

2.3.2 Computational domain and mesh independence analysis

The computational domains for the nine coreholders, as shown in Table 3, were created and spatially discretized in *ANSYS* software. Each of the computer-aided designs of the coreholders consisted of a core plug measuring 7.00 cm in length and 3.82 cm in diameter, placed between the head and end pieces of the same geometry. The computational waterflooding procedure was conducted perpendicularly to the gravity vector.

To ensure the numerical responses are not influenced by the number of cells in the domain, it is necessary to perform a mesh independence analysis. In this study, the procedure proposed by Celik *et al*. (2008) [31] was deemed feasible and was followed. Hence, three meshes for the coreholder equipped with the commercial Spiderweb head/end pieces (case 6 of Table 3) were considered at different levels of refinement. The low refinement mesh contained 76598 elements, while the medium and high refinement domains contained 180331 and 426215 elements, respectively. The number of elements at which the results reached independence was used as a reference value to construct the other domains predicted in Table 3. The main response used to assess mesh independence was the residual oil volume in the core. In Figure 2, the spatial discretization of a coreholder equipped with the Spiderweb headpiece is shown.

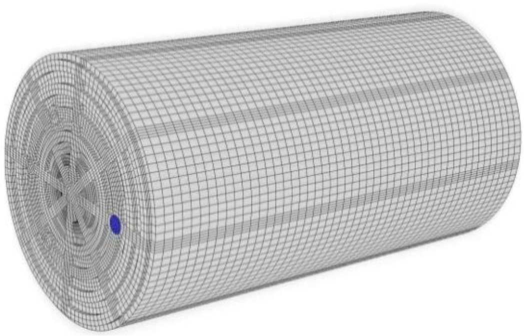

Fig. 2. Computational representation and spatial discretization of coreholder equipped with the commercial headpiece Spiderweb.

3 Results and discussion

3.1 Validation and mesh independence

The validation simulation using the previously presented numerical approach and the experimental data of Santos *et al*. (2021) [27] was performed with a time step of 0.5 s and deemed complete upon reaching steady state. A steady state was considered reached if the difference in means over two consecutive 100 s flow-time intervals for the core's oil volume was less than 0.05 cm^3. This criterion was employed throughout this research.

The steady state was achieved within 1 h of pure brine injection at a flow rate of 1 cm^3/min, which is in good agreement with the experimental data of Santos *et al.* (2021) [27]. The numerical model predicted a residual oil saturation of 0.2608, while the corresponding experimental value was 0.2767, resulting in a relative error of less than 6%. Due to the significant viscosity difference between phases and the complexity of multiphase flow in porous media, it was considered that the numerical approach could reproduce the experimental behavior.

Table 5 presents the oil volume obtained from simulations for the mesh-independence analysis across different computational domains. When following the procedure of Celik *et al*. (2008) [31], it was found that results are no longer influenced by the number of elements in the mesh at an intermediary refinement level. Hence, it was aimed that the total number of elements in the construction of all coreholders meshes foreseen in Table 3 would be approximately 180331.

Table 5. Oil residual volume within the core in the coreholder equipped with the commercial Spiderweb head and end pieces.

Mesh refinement level	Residual oil volume (cm^3)
Low	9.20
Medium	9.42
High	9.34

3.2 Filling pattern

It was observed that brine fills all head geometries following a radial pattern centered at the inlet point. Moreover, it was observed that the bottom of the headpiece fills first, followed by its top, indicating the influence of gravity on the fluids within the headpiece. In Figure 3, the filling pattern of the inlet diffuser of the coreholder in study number 6 of Table 3 is shown, demonstrating the radial filling behavior observed across all devices.

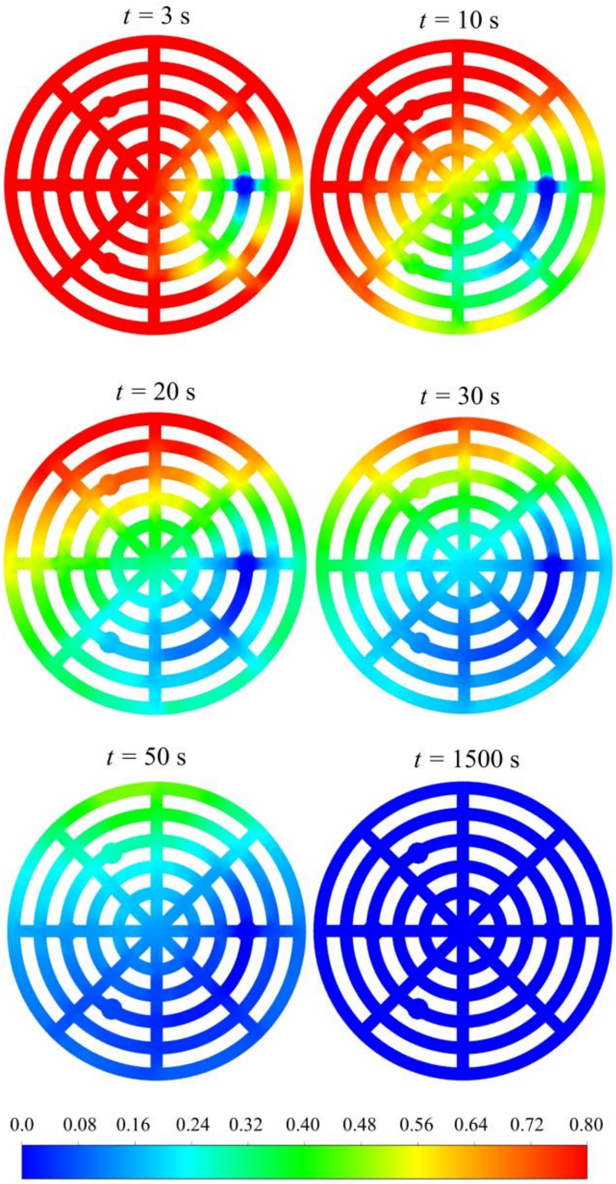

Fig. 3. Phase distribution of oil in the headpiece of the coreholder of study number 6 of Table 3 at different flow times.

When altering the gutter's width of the headpiece, the volume of this section is also changed. Therefore, at a constant injection rate (1 cm^3/min), it is expected that more time will be required to fill the inlet diffuser as its volume increases. This behavior is observed in Figure 4, which shows that at the same flow time of 40 s, more brine has invaded the narrow guttered inlet piece (Figure 4-A).

In contrast, at 40 s of flow time, as the gutter's width increases, it is perceived that larger amounts of oil remain in the headpiece, as shown in Figures 4-B and 4-C.

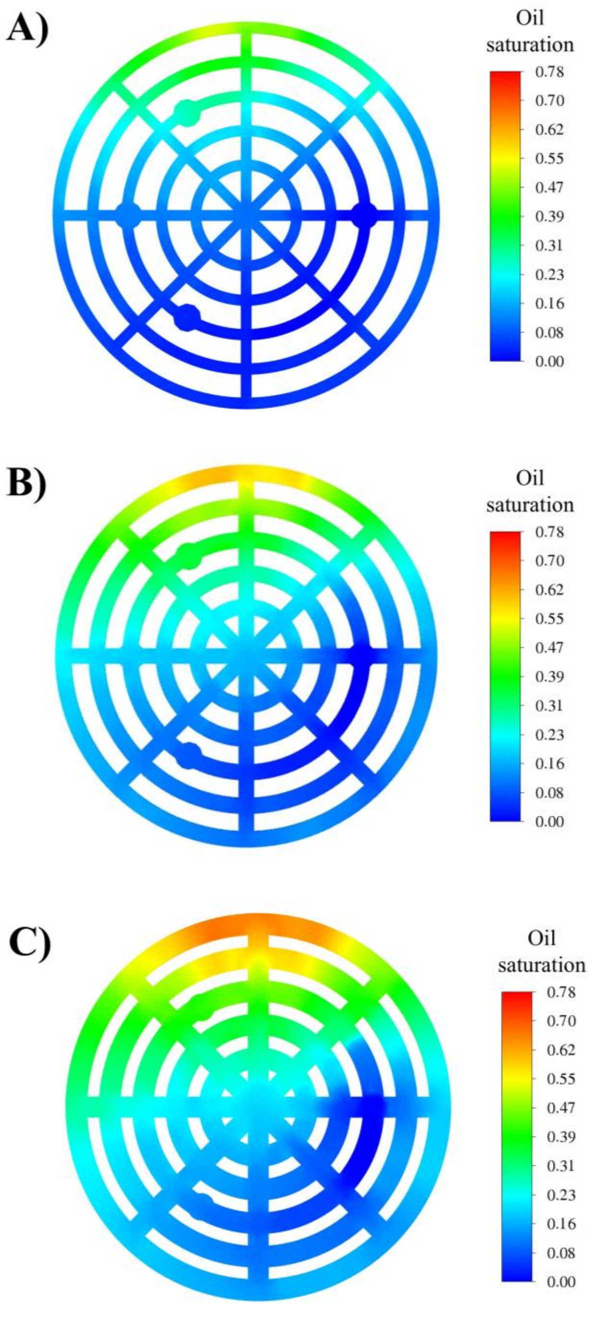

Fig. 4. Phase distribution of oil in the headpiece of the coreholder of study numbers 3 (A), 6 (B), and 9 (C) at 40 s flow time.

Hence, inlet diffusers with narrow gutters could irrigate the totality of the core's face with brine in a shortened time, favoring the formation of a homogeneous front flow. However, as the gutters narrow, the distance between them increases, favoring the development of a phase gradient across sections of the core near the interface between the head diffuser and the plug, thereby impairing the homogeneity of the front flow. Therefore, it is important to set the gutter's width to a value that balances the advantages of rapid filling of the headpiece with tolerable distances between gutters.

3.2 Influence of geometric parameters of the Spiderweb headpiece on the front flow homogeneity

Equations 8 to 10 show how the geometric parameters can influence the average oil saturation in cross-sections near the core's inlet at distances of, respectively, 3 mm, 5 mm, and 10 mm, along with their fitting coefficient of determination (R^2). Equations 8 to 10 were fitted to the steady-state data; hence, they are valid only after this state is achieved. It is demonstrated that the inlet diameter of the headpiece does not influence the saturation of oil in the cross sections considered. This can be justified by demonstrating that this geometrical variable has a small influence on the interface area between the inlet diffuser and the core. For instance, when maintaining the gutter width at 1.00 mm, increasing the inlet diameter from 1.80 mm to 2.60 mm changed the inlet area only from 4.50 cm² to 4.55 cm².

$$S_{O,3mm}(\%) = 16.96 - 8.19X_1 + 0.58X_1X_2 \quad (R^2=0.92) \tag{8}$$

$$S_{O,5mm}(\%) = 26.55 - 11.60X_1 \quad (R^2 = 0.99) \tag{9}$$

$$S_{O,10mm}(\%) = 52.44 - 8.72X_1 \quad (R^2 = 0.92) \tag{10}$$

However, the oil saturation across the analyzed sections was significantly influenced by the width of the headpiece gutters. For example, when increasing this parameter from 1.00 mm to 2.00 mm while maintaining the inlet diameter at 2.60 mm, the interface area between the headpiece and the core increased from 4.50 cm² to 8.20 cm². This enhancement facilitated the penetration of the aqueous phase into the core and the development of a homogeneous front flow near the core's inlet.

This pattern is observed in Figure 5, which shows the saturation of oil in a cross-section 3 mm distant from the core's inlet for cases 3, 6, and 9 of Table 3. Because the inlet diameter is fixed at 2.60 mm, the differences in phase distribution can be attributed solely to changes in channel width.

Respectively, Figures 6 and 7 show that, for cross sections located at 5 mm and 10 mm distant from the core's inlet, a reduction of oil saturation is also observed as the gutter width increases. However, it is perceived that the brine flow front becomes less homogeneous as it moves further from the core inlet.

For the plane 3 mm distant from the core's inlet, a significant oil saturation reduction of 65.19%, on average, was calculated while maintaining the inlet diameter fixed and increasing the gutter's width from 1.00 mm to 2.00 mm. Similarly, average oil saturation reductions of 61.17% and 28.33% were calculated for the cross planes at 5 mm and 10 mm, respectively.

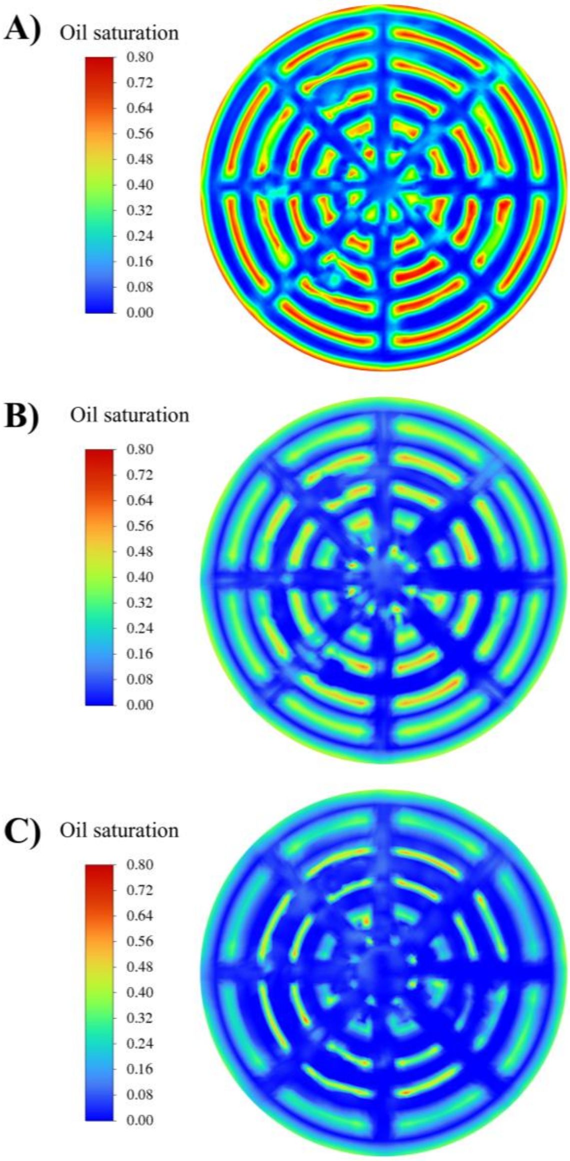

Fig. 5. Phase distribution of oil in a cross-section of the core located 3 mm from the core inlet of study cases number 3 (A), 6 (B), and 9 (C) of Table 3 after 1500 s of flow time.

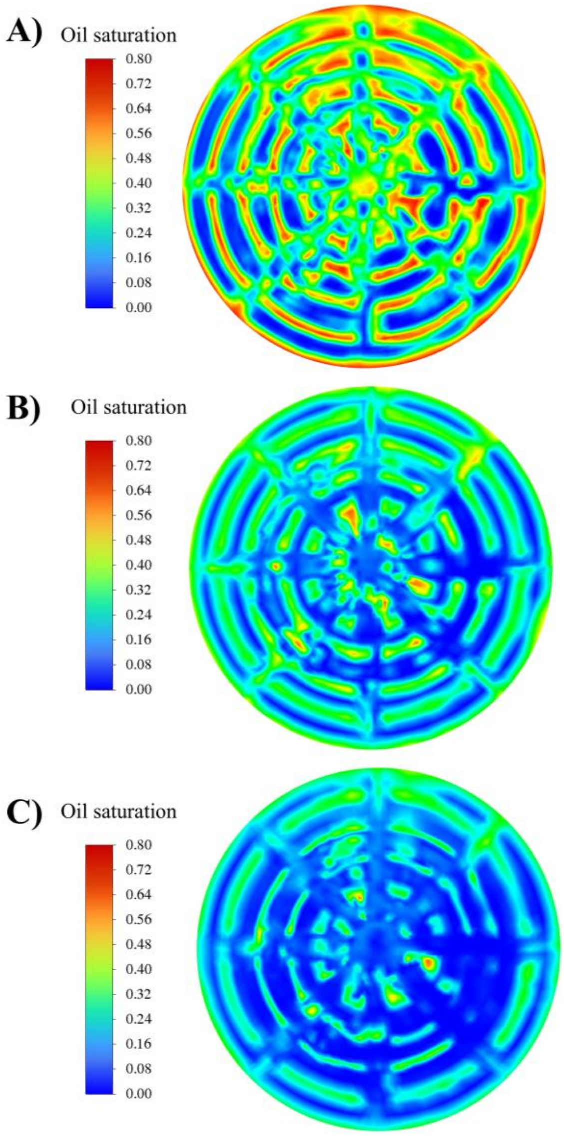

Fig. 6. Phase distribution of oil in a cross-section of the core located 5 mm from the core inlet of study cases number 3 (A), 6 (B), and 9 (C) of Table 3 after 1500 s of flow time.

Figures 5 and 6 also show a clear impression of the headpiece over the cross section of the core, which becomes less evident as the assessed cross plane moves farther from the plug's inlet, as shown in Figure 7. This dynamic discloses that brine starts to flow through a preferred channel.

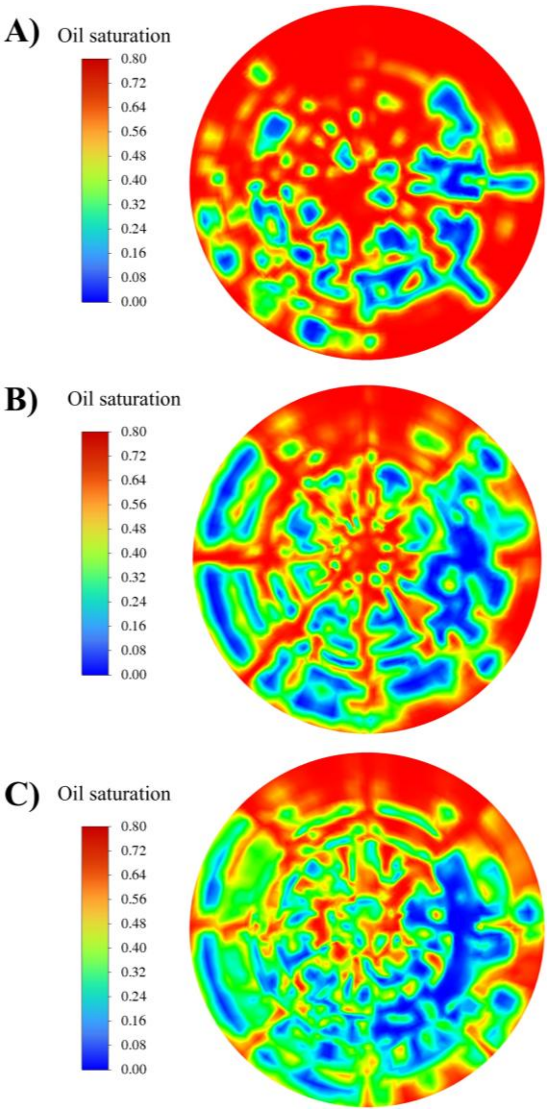

Fig. 7. Phase distribution of oil in a cross-section of the core located 10 mm from the core inlet of study cases number 3 (A), 6 (B), and 9 (C) of Table 3 after 1500 s of flow time.

For the coreholder of study case 6 in Table 3, the phase distribution across a cross-section of the device, with the normal vector parallel to gravity, is presented in Figure 8. In the portion where the brine is admitted into the equipment (left portion of the image), a uniform front flow is observed. However, as brine advances through the plug, protuberances form along the preferential flow path. These dynamics could be explained by the media's moderate permeability and the relatively high brine injection rate used in the waterflooding experiments. This behavior is also observed in all coreholders independent of changes in headpiece design and is in good agreement with other numerical petrophysical studies that employed the VOF multiphase model [12,17,32].

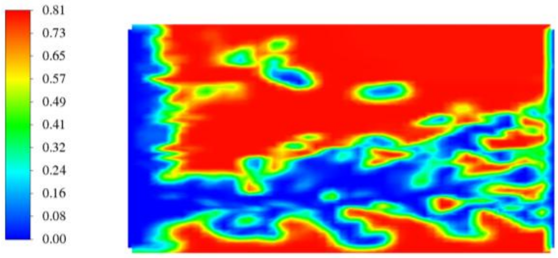

Fig. 8. Phase distribution of oil in a cross-section of the core after 1500 s of flow time.

Although the headpiece design influenced the phase distribution in zones near the core inlet, at the significance level of 0.10, neither of the geometric parameters studied significantly altered the volume of oil extracted from the core; hence, they did not modify its residual saturation. The average residual oil saturation and absolute deviation across all study cases were 59.44% and 2.29%, respectively. The evolution of oil saturation over time at the core of all study cases foreseen in Table 3 is shown in Figure 9, which indicates that a steady state was reached within 1500 s of flow time. Because the inlet geometry does not affect residual oil saturation, the different values observed at the end of each simulation may be attributed to numerical diffusion.

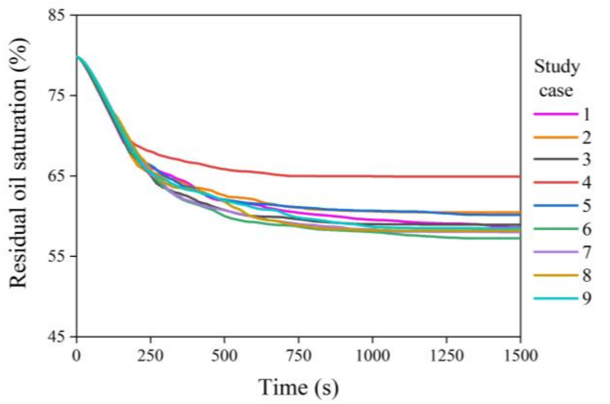

Fig. 9. Phase distribution of oil in a cross-section of the core.

As brine is injected at a single point at the headpiece of the coreholder, its invasion across the core following an axial path from the feeding point is favored. Thereby, the flux of water to regions in the brine front flow that are distant from the input point is hindered; hence, these regions may not display sufficient energy to displace the phases within the core, impeding a piston-like flow of supplied brine.

4 Conclusions

The relative error between the numerical and experimental residual oil saturation values was below 6%. Given the complexity of multiphase flow in porous media, it was assumed that the numerical approach presented in this study could reproduce the waterflooding process. Based on this validated model, statistical tools were used to investigate how the geometry of the headpiece could alter the brine front flow across the core. Within the range of the geometrical variables studied, the inlet diameter did not influence any of the analyzed responses, as it had little effect on the area through which the brine flows from the diffuser to the core. In contrast, the gutter width had a pronounced effect on the flow distribution near the inlet. Increasing the gutter width from 1.00 mm to 2.00 mm, while maintaining a constant inlet diameter, increased oil displacement by 65.19%, 61.17%, and 28.33% at cross sections located 3 mm, 5 mm, and 10 mm from the interface of the headpiece and core, respectively.

Acknowledgments

The authors would like to thank PETROBRAS (Petróleo Brasileiro S.A.) for funding and support, as well as UFRRJ and the Fluid Flow Laboratory for its support in developing this work.

References

1. R. Alali, K. Abe, and H. Fujii, ACS Omega **10**, 15967 (2025).

2. M. Seidy-Esfahlan, S. A. Tabatabaei-Nezhad, and E. Khodapanah, Heliyon **10**, e37826 (2024).

3. T. Acharya, L. Song, E. Duginski, and A. Goodwin, Processes **11**, 1 (2023).

4. P. Bikkina, J. Wan, Y. Kim, T. J. Kneafsey, and T. K. Tokunaga, Fuel **166**, 219 (2015).

5. H. Luo, M. Delshad, G. A. Pope, and K. K. Mohanty, J. Pet. Sci. Eng. **165**, 332 (2018).

6. N. Hemmati, S. Borazjani, S. Yang, A. Badalyan, L. Genolet, A. Behr, A. Zeinijahromi, and P. Bedrikovetsky, Fuel **321**, 123940 (2022).

7. R. Gupta, R. Longoria, J. D. Spitzenberger, D. C. Laverick, and C. A. Crowell, US 2017 / 0248506 A1 (2017).

8. S. Yang, N. Hemmati, T. Russell, A. Zeinijahromi, S. Borazjani, A. Behr, L. Genolet, and P. Bedrikovetsky, J. Pet. Sci. Eng. **208**, 109533 (2022).

9. M. Shakerian, F. Marica, A. Afrough, F. G. Goora, M. Li, S. Vashaee, B. J. Balcom, M. Shakerian, F. Marica, A. Afrough, F. G. Goora, M. Li, and S. Vashaee, Rev. Sci. Instrum. **88**, (2017).

10. S. Mohammadi, Heliyon **10**, (2024).

11. A. Jafari, M. Hasani, M. Hosseini, and R. Gharibshahi, Pet. Sci. **17**, 434 (2020).

12. A. Pinilla, L. Ramirez, M. Asuaje, and N. Ratkovich, Fuel **287**, (2021).

13. S. K. Nandwani, M. Chakraborty, and S. Gupta, J. Pet. Sci. Eng. **173**, 835 (2019).

14. M. F. Mehraban, P. Rostami, S. Afzali, Z. Ahmadi, M. Sharifi, and S. Ayatollahi, J. Pet. Sci. Eng. **191**, 107149 (2020).

15. R. M. McDavid, in edited by K. H. J. Buschow, R. W. Cahn, M. C. Flemings, B. Ilschner, E. J. Kramer, S. Mahajan, and P. B. T.-E. of M. S. and T. Veyssière (Elsevier, Oxford, 2001), pp. 4720–4732.

16. F. Garoosi, A. Kantzas, and M. Irani, Eng. Anal. Bound. Elem. **166**, (2024).

17. S. K. Nandwani, N. Saxena, and A. Kumar, J. Mol. Liq. **396**, 124112 (2024).

18. Y. Xue, C. Guo, X. Gu, Y. Xu, L. Xue, and H. Lin, Micromachines **12**, 1 (2021).

19. H. Xie, D. Liang, H. Peng, X. Wei, J. Zhao, J. Fu, and J. Zhang, Energy **334**, 137728 (2025).

20. U. ANSYS Inc., ANSYS Inc., USA (2025).

21. J. U. Brackbill, D. B. Kothe, and C. Zemach, J. Comput. Phys. **100**, 335 (1992).

22. M. Azhar and J. Sanyal, Proc. 4th World Congr. Momentum, Heat Mass Transf. 1 (2019).

23. W. Zhong, X. Ji, C. Li, J. Fang, and F. Liu, Appl. Sci. **8**, (2018).

24. P. Horgue, C. Soulaine, J. Franc, R. Guibert, and G. Debenest, Comput. Phys. Commun. **187**, 217 (2015).

25. J. Foroozesh and M. Jamiolahmady, Fuel **184**, 581 (2016).

26. G. S. Beavers, E. M. Sparrow, and D. E. Rodenz, J. Appl. Mech. Trans. ASME **40**, 655 (1973).

27. I. Santos, E. FM, N. DSS, C. J. CR, and P. Couto, Pet. Petrochemical Eng. J. **5**, (2021).

28. W. Seok, G. H. Kim, J. Seo, and S. H. Rhee, J. Mar. Sci. Eng. **7**, (2019).

29. J. Choi, H. Cho, Y. Choi, and S. Lee, Desalination **524**, 115460 (2022).

30. K. Elsayed and C. Lacor, Appl. Math. Model. **37**, 5680 (2013).

31. I. B. Celik, U. Ghia, P. J. Roache, C. J. Freitas, H. Coleman, and P. E. Raad, J. Fluids Eng. Trans. ASME **130**, 0780011 (2008).

32. F. J. Carrillo, I. C. Bourg, and C. Soulaine, J. Comput. Phys. X **8**, 100073 (2020).